Explicit Solvent DRF INDOs/CIS Computations of Charge Transfer State Energetics in a Pyrenyldeoxyuridine Nucleoside Model

Piet Th. Van Duijnen[†] and Thomas L. Netzel*[,‡]

Theoretical Chemistry, Materials Science Centre, Rijksuniversiteit Groningen, Nijenborgh 4, 9747 AG Groningen, Netherlands, and Department of Chemistry, Georgia State University, P.O. Box 4098, Atlanta, GA, 30302-4098

Received: July 29, 2005; In Final Form: November 18, 2005

In this work we present calculated absorption and emission spectra in acetonitrile (MeCN) solution of *N*-acetyl-1-aminopyrene (PAAc, a spectroscopic model compound) and *N*-(1-pyrenyl)-1-methyluracil-5-carboxamide (PAU_{Me}, a computational model for 5-(*N*-carboxyl-1-aminopyrenyl)-2′-deoxyuridine (PAdU)). The computational method used—the discrete reaction field approach (DRF)—combines a quantum mechanical (QM) description of the solute (here DFT and INDOs/CIS, i.e., the INDO parametrization for spectroscopy) with a classical, molecular mechanics (MM) description of the solvent molecules. The latter are modeled with point charges representing the permanent charge distribution and polarizabilities to account for many-body interactions among the solute and other solvent molecules. Molecular dynamics is used to sample the degrees of freedom of the solution around several solute conformations each in two electronic excited states. This leads to a large number of solute/solvent configurations from which 800 are selected for each excited state and collected into a single ensemble by means of proper Boltzmann averaging. DRF INDOs/CIS applied to the selected solute/solvent configurations give simulated absorption and emission band spectra—each based on 15 200 calculated transitions—that compare well with experimental results. For example, the much broader absorption and emission bands in PAdU compared with PAAc are reproduced, and the simulated emission spectra of PAU_{Me} agree well with broad (380−550 nm) charge transfer (CT) emission seen for PAdU in MeCN. The observed multiexponential fluorescence decay profiles for PAdU in different polar solvents are interpreted in terms of solute/solvent conformational heterogeneity here generated in the MD simulations for PAU_{Me} in MeCN. Additionally, the simulations demonstrate the mixing of the forbidden $Py^{\bullet+}/dU^{\bullet-}$ CT states with allowed pyrenyl $^1(\pi,\pi^*)$ states.

Introduction

The spectroscopy of 5-(N-carboxyl-1-aminopyrenyl)-2′-deoxyuridine (PAdU; see Figure 1) in tetrahydrofuran (THF), methanol (MeOH) and acetonitrile (MeCN)[1] has several remarkable features, the most important being the extensive quenching of the photoexcited $^1(\pi,\pi^*)$ state of its pyrenyl chromophore relative to *N*-acetyl-1-aminopyrene (PAAc—a spectroscopic model compound). Stronger pyrenyl emission quenching in the more polar solvents MeCN and MeOH compared to that seen in the less polar solvent THF is consistent with the proposal that the photophysics is controlled by the formation of intramolecular $Py^{\bullet+}/dU^{\bullet-}$ charge transfer (CT) excited states.

Earlier efforts to elucidate the solvent dependence of intramolecular CT quenching of pyrenyl emission in pyrenyl-dU nucleosides by means of INDOs/CIS, i.e., the INDO parametrization for spectroscopy and wave function expansions in terms of determinants obtained from single excitation transitions only,[3] quantum chemical calculations on PAAc and a computational model for PAdU (PAU_{Me}; see Figure 1), were only partly satisfying in the sense that gas phase calculations[1] indicated that the relative energy and dipole moment of $Py^{\bullet+}/dU^{\bullet-}$ CT states depended on PAU_{Me} conformation and that in all conformers the lowest energy CT states were much higher than the lowest energy pyrenyl $^1(\pi,\pi^*)$ excited states. A second computational study[2] addressed the solvent effects by applying the self-consistent reaction field (SCRF)[4] in which the solute was placed inside a spherical cavity in a dielectric continuum with (dielectric constant) $\epsilon = 40$, presumably mimicking MeCN as the solvent. This work showed that the ordering of CT states in solution differed widely from the gas phase situation and that CT excited states with large dipole moments could easily be lower in energy than the lowest energy pyrenyl $^1(\pi,\pi^*)$ excited states. However, SCRF results depend heavily on the cavity radius that is at best an empirical parameter. Moreover, they are quantitatively doubtful because the only source of the

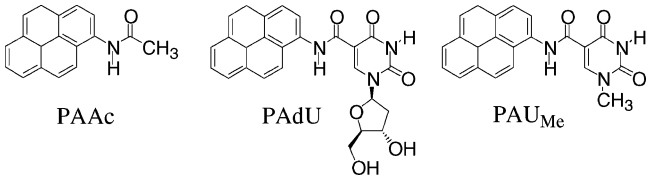

Figure 1. Structural drawings of the pyrenyl ligand spectroscopic model, PAAc, the pyrenyl substituted 2′-deoxyuridine nucleoside, PAdU, and the computational model of the pyrenyl nucleoside, PAU_{Me}. Note that all eight PAU_{Me} conformers investigated in this work were in the more stable trans-amido conformation shown in this figure and were the identical to the trans-amido conformers in Mitchell et al.[2]

* Corresponding author. Phone/Fax: (404)-651-3129. Home phone: (404)-633-7390. E-mail: tnetzel@gsu.edu.
[†] Rijksuniversiteit Groningen.
[‡] Georgia State University.

10.1021/jp0542221 CCC: $33.50
Published on Web 01/26/2006

reaction field is the solute's dipole moment (Onsager model[5]), thus neglecting most of the details of the solute's charge distribution. Additionally, the reaction potential depends approximately on $(\epsilon - 1)/(2\epsilon + 1)$, which is within 6% constant for $20 < \epsilon < 100$. In reality, for very different solvents with about the same ϵ, the effects of solvation may in fact be very different, yet within a dielectric continuum model the solvation effects will come out almost the same. SCRF calculations are cheap, but the results should be considered as qualitative. Finally, the solute-in-cavity model yields only single transitions (stick spectra) and does not describe solvent broadening.

In this work these INDOs/CIS exercises were repeated with a discrete reaction field (DRF) solvation model in which the MeCN solvent was represented by discrete molecules that were characterized by (atomic) charges, polarizabilities, and radii. Molecular dynamics (MD) or Monte Carlo (MC) techniques could be used to equilibrate solvent around the charge distribution of the solute (or, rather a classical representation of that distribution) in any electronic state. The advantages are many: no unphysical parameters, ample attention to microscopic detail, and inclusion of specific solute/solvent interactions such as hydrogen bonding. The only disadvantage is that the discrete solvent model was computationally more demanding than the dielectric continuum model; true for the greater part because of the need for MD or MC simulations. Earlier, the DRF solvation model had been used successfully in spectroscopy related studies with ab initio,[6,7] DFT,[8,9] and INDOs/CIS.[10] Here the DRF solvation model was used, in combination with INDOs/CIS[3] to generate simulated absorption and emission (band) spectra for PAAc and PAU_{Me} in MeCN. In particular, the latter QM method was applied to these solutes to rationalize and quantify previously reported spectroscopic results for the PAdU nucleoside in MeCN.

In the following sections we will summarize the spectroscopic findings for PAdU, describe the DRF solvent model and its implementation for INDOs/CIS, compare calculated and experimental spectra of PAAc and, respectively, for PAU_{Me} and PAdU, show the effects of solvent reorganization on the electronic properties of $Py^{\bullet+}/dU^{\bullet-}$ CT excited states, and end with some concluding remarks.

Background

Experimental PAdU Excited State Dynamics. Previous spectroscopic investigations of the pyrenyl-dU nucleoside, PAdU, in deoxygenated THF, MeCN, and MeOH solvents established three main points.[1] One, the initial photoexcited $^1(\pi,\pi^*)$ state of the pyrenyl chromophore is extensively quenched relative to a model pyrenyl compound that cannot undergo intramolecular CT, *N*-acetyl-1-aminopyrene (PAAc): 95% (THF), 96% (MeCN), and 99% MeOH. Additionally, the pyrenyl emission quenching is larger in the more polar solvents (MeCN and MeOH) than in the less polar solvent THF, as expected if the quenching is due to intramolecular CT. Two, the PAdU nucleoside emits from the $Py^{\bullet+}/dU^{\bullet-}$ CT state in all three of the above solvents in the 500−600 nm range to the red of the 370−465 nm emission range for the $^1(\pi,\pi^*)$ state of the pyrenyl chromophore. The red, CT emission is broad and structureless, whereas emission from the pyrenyl $^1(\pi,\pi^*)$ state shows vibrational structure due to C−C stretching; additionally, the emission lifetime of the CT product is short, ≤100 ps.

The third important point is that the pyrenyl emission exhibits up to three apparent decay lifetimes in the ≤100-ps to 25 ns time range. In MeCN, for example, the emission kinetics of PAdU in the pyrenyl and CT regions are qualitatively similar to those in MeOH with up to 33% of the pyrenyl emission at 415 and 440 nm decaying with two lifetimes in the 3−5 and 10−13 ns time ranges. The multiexponential emission decay of the pyrenyl chromophore in MeOH and MeCN in the 370−465 nm regions arises from conformational heterogeneity within solutions of the PAdU nucleoside on time scales of 25 ns or less. In particular, the pyrenyl $^1(\pi,\pi^*)$ states of different conformers undergo intramolecular CT to form the $Py^{\bullet+}/dU^{\bullet-}$ CT state with a wide variety of lifetimes spanning ≤100 ps to 25 ns.

A recent femtosecond transient absorption (TA) study of PAdU in MeCN and MeOH confirms the earlier $Py^{\bullet+}/dU^{\bullet-}$ CT state dynamics assignments based on emission quantum yield and kinetics measurements.[11] The key result is that the TA spectra seen in the 0.6−20 ps time range for PAdU in both MeCN and MeOH have a strong broad absorption maximum at 520−540 nm with a weak shoulder at 560−580 nm. The wavelengths of these TA maxima are intermediate between those of the $Py^{\bullet+}/dU^{\bullet-}$ CT states of 5-(pyren-1-yl-carbonyl)-2′-deoxyuridine (PCOdU) at 460 nm in MeOH[12] and of 5-(pyren-1-yl)-2′-deoxyuridine (PdU) at 590 nm in phosphate buffer.[13,14] Surprisingly, in view of the triexponental pyrenyl $^1(\pi,\pi^*)$ emission lifetimes discussed above, all evidence of pyrenyl $^1(\pi,\pi^*)$ states is masked in the TA spectra of PAdU by the strong CT product absorption until the CT products back-react with average lifetimes of 5.3 and 6.0 ps, respectively, in MeCN and MeOH. Within the 20 ps to 1 ns TA time window, slowly quenched pyrenyl $^1(\pi,\pi^*)$ states decay with an apparent lifetime of ca. 2.6 ns in both MeCN and MeOH. This later TA relaxation agrees well with previously found pyrenyl $^1(\pi,\pi^*)$ emission lifetimes in the 3−5 ns time range (ca. 25% amplitude in MeCN and 1−5% amplitude in MeOH).[1] Combining emission quantum yield and lifetime results with these new TA observations, allows us to draw the following overall picture of the photophysical processes for PAdU in MeCN. Approximately, 96% of the pyrenyl $^1(\pi,\pi^*)$ states of PAdU are quenched (on the basis of relative emission quantum yields) within 600 fs of photoexcitation to produce the $Py^{\bullet+}/dU^{\bullet-}$ CT state. This CT state then back-reacts to produce apparently exclusively the ground state of PAdU with an average lifetime of 5.3 ps. In parallel with these forward and reverse, intramolecular CT processes characteristic of most PAdU conformers, approximately 4% of the PAdU nucloside conformers in MeCN undergo CT quenching of their $^1(\pi,\pi^*)$ states in the 3−13 ns time range. Presumbly, the back reaction times for these slowly formed CT products are also only ca. 5 ps. Thus TA kinetics experiments would not observe them following the decay of the nanosecond-lived $^1(\pi,\pi^*)$ states. TA spectral and kinetics results for PAdU in MeOH are remarkably similar to those for PAdU in MeCN.

Figure 2 summarizes the kinetics events following photoexcitation of a solution of PAdU nucleoside in MeCN and highlights the fact that PAdU exists as an ensemble of different conformers each with a variety of solvent configurations. Strikingly, the energy of the $Py^{\bullet+}/dU^{\bullet-}$ CT states of most conformers in most solvent environments is too high to permit CT immediately following light absorption.[1,2] This is true because the solvent configuration immediately following photoexcitation is the same as that of the nucleoside's ground state (Frank Condon principle). For very polar excited states (such as most $Py^{\bullet+}/dU^{\bullet-}$ CT states) in polar solvents, solvent orientation has a very large effect on excited state energy. Note that emission from CT_1 states with CT-equilibrated solvent (red levels) will terminate in S_0 states also with CT-equilibrated solvent. These latter S_0 states will be higher in energy than the

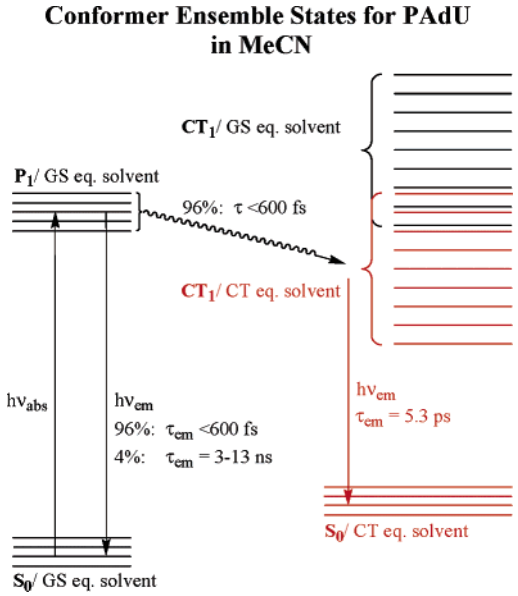

Figure 2. Electronic energy level diagram for an ensemble of PAdU conformers in MeCN. S_0 is the ground state (GS), P_1 is the lowest energy pyrenyl $^1(\pi,\pi^*)$ state, and CT_1 is the lowest energy $Py^{\bullet+}/dU^{\bullet-}$ charge transfer state. The indicated emission and CT_1 formation lifetimes (τ) are discussed in the text. Importantly, the multiple levels for each state represent multiple electronic origins arising from different PAdU conformers each with numerous solvent configurations. The dispersion of electronic origins is much larger for the CT_1 states than for the S_0 and P_1 states and depends strongly on whether the solvent surrounding the CT_1 state is equilibrated with the charge distribution of the ground (GS eq. solvent) or CT_1 (CT eq. solvent) state.

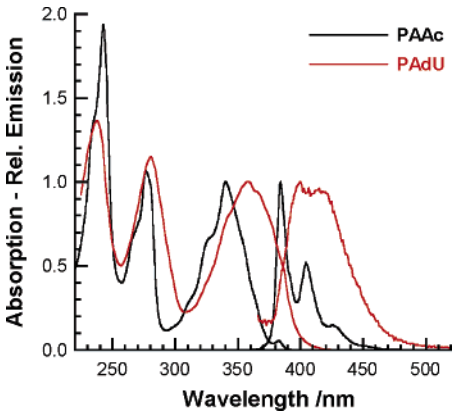

Figure 3. Normalized absorption and emission spectra for PAAc and PAdU in MeCN. Data taken from Kerr et al.[1]

corresponding S_0 states with GS-equilibrated solvent. Figure 2 tacitly ignores energy differences between P_1 and S_0 states with P_1-equilibrated solvent (the states responsible for pyrenyl emission) and the same states with GS-equilibrated solvent (the states responsible for pyrenyl absorption). However, the small Stokes shift seen in Figure 3 (ca. 1.5 nm) between the absorption and emission origins for PAAc in MeCN justifies this neglect. Thus both the increased energy of S_0 states and the decreased energy of CT_1 states with CT-equilibrated solvent (compared to the corresponding states with GS-equilibrated solvent) are responsible for the much lower energy of the $Py^{\bullet+}/dU^{\bullet-}$ CT emission seen in MeCN for the PAdU nucleoside compared to the pyrenyl emission seen for the PAAc spectroscopic model in the same solvent (see Figure 3).

Theory and Computational Procedures

Discrete Reaction Field Approach. In the DRF[15−18] approach a solute is described by some quantum mechanical (QM) method (the QM system), whereas the solvent is modeled via molecular mechanics (MM) by any number of discrete molecules and—optionally—an enveloping dielectric continuum (the MM system). The permanent charge distribution of a solvent molecule is represented by point charges, mainly at the constituent atoms, but more sites may be used to represent multipole monents beyond the dipole moment. The needed charges are obtained from appropriate quantum chemical calculations.[19,20] Changes in the charge distribution, due to interactions with other parts of the system, are taken care of by putting polarizabilities located either at the atoms (distributed polarizability model) or at appropriate centers (group polarizability model). Polarizabilities are obtained from appropriate quantum chemical calculations or from fitting to experimental results.[21−23]

Thus, the (effective) Hamiltonian of the complete system ($\hat{H}$) is written as

$$\hat{H} = \hat{H}_{QM} + \hat{H}_{QM/MM} + \hat{H}_{MM} \quad (1)$$

where $\hat{H}_{QM}$ is the solute's quantum mechanical Hamiltonian, $\hat{H}_{MM}$ is the classical Hamiltonian of the classical solvent, and $\hat{H}_{QM/MM}$ describes the solute/solvent interactions. Within the DRF approach the QM/MM operator ($\hat{H}_{QM/MM}$) at a point r_i is in general given by

$$\hat{H}_{QM/MM}(r_i) = \hat{v}^{DRF}(r_i) = \hat{v}^{es}(r_i) + \hat{v}^{pol}(r_i) + \hat{v}^{rep}(r_i) \quad (2)$$

where $\hat{v}^{es}$ is the electrostatic operator describing the Coulombic interaction between the QM solute and the static charge distribution of MM solvent, $\hat{v}^{pol}$ is the polarization operator describing the many-body polarization of the solvent molecules, i.e., the changes in the charge distribution of these molecules due to interactions with the QM solute and other parts of the MM solvent, and $\hat{v}_{rep}$ is the (model) Pauli repulsion term that is important only for molecular dynamics (MD) as it does not affect electrons. For details see, for example, de Vries et al.[17]

Because the solvent charge distribution is represented by point charges, the electrostatic operator is simply

$$\hat{v}^{es}(r_i) = \sum_s \frac{q_s}{R_{si}} = \sum_s q_s T^{(0)}_{si} \quad (3)$$

where the index s runs over all charged sites in the solvent, and we introduce the zeroth-order tensor. The general form of the interaction tensors to a given order n is

$$T^n_{pq,\alpha_1\cdots\alpha_n} = \nabla_{pq,\alpha_1} \cdots \nabla_{pq,\alpha_n}\left(\frac{1}{R_{pq}}\right) \quad (4)$$

with R_{pq} the distance between sites p and q. We note that without the QM solute, eqs 1 and 2 define a classical polarizable force field.[24]

Many-Body Polarization. The many-body polarization operator is given in the form of the induced dipoles at the polarizable sites

$$\hat{v}^{pol}(r_i) = \sum_s \vec{\mu}^{ind}_{s,\alpha} T^{(1)}_{si,\alpha} \quad (5)$$

where $R_{si,\alpha}$ is a component of the distance vector, and $\vec{\mu}^{ind}_{s,\alpha}$ is

the induced dipole at site s. For Greek indices the Einstein summation is employed.

For a collection of polarizabilities in an electric field $\vec{F}^{\text{init}}$, the induced moment at s is given by

$$\vec{\mu}^{\text{ind}}_{s,\alpha} = \alpha_{s,\alpha\beta}[\vec{F}^{\text{init}}_{s,\beta} + \sum_{s\neq t} T^{(2)}_{st,\beta\gamma}\vec{\mu}^{\text{ind}}_{t,\gamma}] \quad (6)$$

with $\alpha_{s,\alpha\beta}$ a component of the polarizability at s, and the dipole field is given by

$$T^{(2)}_{st,\alpha\beta} = \frac{3R_{st,\alpha}R_{st,\beta}}{R_{st}^{\ 5}} - \frac{\delta_{\alpha\beta}}{R_{st}^{\ 3}} \quad (7)$$

Equation 6 can be solved self-consistently by rewriting it into a $3M \times 3M$ linear matrix equation for M polarizabilities as

$$\overleftrightarrow{A}\vec{\mu}^{\text{ind}} = \vec{F}^{\text{init}} \quad (8)$$

with the components of $\overleftrightarrow{A}$ defined as

$$A_{st,\alpha\beta} = (\alpha_{st,\alpha\beta}^{\ -1} - T^{(2)}_{st,\alpha\beta}) \quad (9)$$

The matrix

$$\overleftrightarrow{B} = \overleftrightarrow{A}^{-1} \quad (10)$$

(also known as the *relay matrix*) is a generalized many particle polarizability as in

$$\vec{\mu}^{\text{ind}} = \overleftrightarrow{B}\vec{F}^{\text{init}} \quad (11)$$

The matrixes $\overleftrightarrow{A}$ are usually constructed following the procedure of Thole[21] or equivalently that of Swart et al.[25] in which at short distances inducing fields and interactions between induced dipoles are damped to avoid unphysical polarization.

Matrix Elements and Energies. Because wave functions within the INDO method[3,26,27] are expanded in terms of basis functions, all expectation values are obtained as linear combinations of integrals. Details of their evaluation are given elsewhere.[17]

Without an external field, $\vec{F}^{\text{init}}$ in eq 6 is given by

$$\vec{F}^{\text{init}}_{s,\alpha} = \vec{F}^{\text{QM,el}}_{s,\alpha} + \vec{F}^{\text{QM,nuc}}_{s,\alpha} + \vec{F}^{\text{MM}}_{s,\alpha} \quad (12)$$

with

$$\vec{F}^{\text{QM,el}}_{t,\beta} = \langle\Psi|\sum_{s\neq t}(-T_{st,\beta}^{\ (1)})|\Psi\rangle$$

$$\vec{F}^{\text{QM,nuc}}_{t,\beta} = \sum_m Z_m(-T_{mt,\beta}^{\ (1)})$$

$$\vec{F}^{\text{MM}}_{t,\beta} = \sum_s{}' q_s(-T_{st,\beta}^{\ (1)}) \quad (13)$$

where Ψ stands for the actual state of the QM solute, Z_m is the nuclear charge of atom m, q_s is the electronic charge on site s, and the prime in the last sum indicates that in eq 8 polarization within the same classical group is excluded. We note that the contribution of $\vec{F}_{t,\beta}^{\text{MM}}$ to $\hat{v}^{\text{pol}}$ gives, for a single solvent configuration, just an additional term to the static potential.

For the evaluation of the polarization energy we calculate the *total* field of eq 12, generate the induced dipoles of eq 5 by solving eq 11, and then construct the operator $\hat{v}^{\text{pol}}$ for this field for each SCF iteration. Effectively, this just generates another external potential. For this average reaction field (ARF) approach, an effective one-electron operator is constructed as

$$h^{\text{ARF}}_{pq} = (\langle\vec{F}^{\text{QM,el}}\rangle + \vec{F}^{\text{QM,nuc}} + \vec{F}^{\text{MM}})\vec{B}\hat{v}^{\text{pol}}_{pq} = \langle\vec{M}^{\text{ind}}\rangle\hat{v}^{pol}_{pq}$$
$$(p,q \in \text{basis functions}) \quad (14)$$

for which only a set of one-electron integrals of $\hat{v}^{\text{pol}}$ over the basis functions is needed.

The contribution to the energy of the total system is

$$\Delta U^{\text{ARF}} = {}^1/_2\{\langle h^{\text{ARF}}\rangle + \langle\vec{M}^{\text{ind}}\rangle\langle\vec{F}^{\text{QM,nuc}} + \vec{F}^{\text{MM}})\} \quad (15)$$

Obviously, this case accounts only for electrostatic interactions.

Implementation of DRF INDO. We have implemented the DRF for single determinant (RHF, ROHF and UHF) wave functions with the standard INDO parametrization (DRF INDO).[26,27] Because INDO is intrinsically a minimal basis set approach, we use expanded electric fields and (reaction) potentials for evaluating $\hat{H}_{\text{QM/MM}}$ with the solute's nuclei and the center of mass of the solute as expansion centers; thus all needed integrals can be obtained as linear combinations of overlap and dipole integrals.[17] We note that for the parametrization in INDO it is assumed that the basis set is (Löwdin) orthogonalized. In contrast, the interaction integrals for $\hat{H}_{\text{QM/MM}}$ need to be evaluated in the nonorthogonal Slater basis set. This requires in various places transformations from the Löwdin basis set to the Slater basis set and vice versa. By default, no two-electron DRF integrals are computed for the SCF ground state, because we use the ARF formulation. Thus the dispersion interactions are not calculated. For calculating spectra we apply INDOs/CIS.

For closed shell ground wave functions, this DRF INDO procedure is relatively simple. RHF calculations give ground state Hartree−Fock orbitals and their corresponding eigenvalues as

$$\epsilon_i = \langle i|h_1|i\rangle + \langle ij|h_2|ij\rangle + \langle i|h^{\text{ARF}}_{\text{gs}}|i\rangle \quad (16)$$

with h_1 and h_2, respectively, the standard one- and two-electron operators, i and j (molecular) orbital indices, and $h^{\text{ARF}}_{\text{gs}}$ the reaction field operator constructed from the ground state density. Thus to evaluate $\Delta E(i\rightarrow k)$, first the difference density $\Delta D_{i\rightarrow k}$ for state $\Psi(i\rightarrow k)$ is constructed from which we obtain

$$\Delta(h^{\text{ARF}}_{\text{gs}})_{i\rightarrow k} = \langle k|(h^{\text{ARF}}_{\text{gs}})|k\rangle - \langle i|(h^{\text{ARF}}_{\text{gs}})|i\rangle = \text{trace}[\Delta D_{i\rightarrow k}h^{\text{ARF}}_{\text{gs}}] \quad (17)$$

to remove the ground state contribution of $h^{\text{ARF}}_{\text{gs}}$ to this orbital energy. Then with the density of state $\Psi(i\rightarrow k)$, we finally have

$$\Delta E_{i\rightarrow k} = \epsilon_k - \epsilon_i + \Delta h^1_{i\rightarrow k} + \Delta' h^2_{i\rightarrow k} - \Delta(h^{\text{ARF}}_{\text{gs}})_{i\rightarrow k} + {}^1/_2\langle h^{\text{ARF}}_{i\rightarrow k}\rangle_{i\rightarrow k} \quad (18)$$

These steps are formally the same as those used earlier by Karelson and Zerner.[4]

Computational Procedures. For PAAc we examined eight conformers obtained by rotating the *N*-acyl group in steps of 45° from the fully planar structure. The latter was replaced by the gas phase optimized structure. For PAU_{Me} we took eight conformers each at a local energy minimum from a previous SCRF INDOs/CIS study.[2] Each of the conformers was subject to a DFT calculation using the Amsterdam Density Functional[28] (ADF) package for generating the heats of formation. The resulting heats of formation showed that all of the conformers for both compounds were thermally accessible.

Separate classical MD simulations were performed for each conformer immersed in 100 MeCN molecules using the DRF90 program[24] with rigid solute and solvent molecules and a time step of 1 fs at a temperature of 298 K controlled by a Nosé−Hoover thermostat[29] in an *NVT* ensemble. The molecules were placed in a (virtual) sphere with a radius of about 28 bohr, and a soft wall-force[25] was applied to keep the molecules from evaporating. Equilibration runs of about 20 ps were performed, followed by 50 ps production runs from which 100 uncorrelated solute/solvent configurations were selected and saved. This is sufficient to retain all statistically significant solute/solvent information.[30] In fact, two series of such MD simulations were run for each conformer, one for the solvent equilibrated with respect to the conformers' ground state charge distribution and the other for the solvent equilibrated with respect to the first (vacuum) $Py^{\bullet+}/dU^{\bullet-}$ CT excited state for PAU_{Me} conformers and to the first (vacuum) $^1(\pi,\pi^*)$ excited state for PAAc conformers.

From the first MD series, we used DRF INDOs/CIS to calculate the energies of the 20 lowest energy electronic states, their dipole moments, and the oscillator strengths connecting them with the ground state. By scaling each conformer's oscillator strengths with Boltzmann factors obtained by combining the ADF vacuum energies and the classical MD energies for each solvated conformer, we were able to consider the 800 saved configurations as belonging to a single ensemble. We created ensemble absorption spectra for each compound by adding the Boltzmann weighted oscillator strengths for each family of conformers in 200 intervals of equal energy-width over a wavelength region from about 200 to 370 nm. Emission spectra were calculated similarly, but without Boltzmann weighting, from the second MD series using only either the lowest energy excited state or the two lowest energy excited states.

In the MD simulations the solutes' charge distributions were represented by atomic effective charges from the corresponding vacuum INDO calculations. INDO atomic charges reproduce the dipole moments of electronic states fairly well. Although ADF calculations generate better point charges[20] for the ground state, they do not describe excited states very well. Thus, for consistency we applied INDO charges throughout this work.

In summary, for each compound and for both absorption and emission spectra, 800 statistically significant solute/solvent configurations (based on eight different solute conformers) were obtained and used to calculate 20 electronic excited states. Consequently, each simulated band spectrum here is based on 15 200 computed transitions.

Results and Discussion

Absorption and Emission Spectra for PAAc and PAdU in MeCN. Figure 3 presents plots of the absorption and emission spectra in MeCN for the PAdU nucleoside and PAAc, a pyrenyl spectroscopic model. The PAAc model has close to normal pyrenyl spectroscopic features. In absorption, a reasonably forbidden S_1 electronic origin band at 383 nm and very strong S_2 absorption features at 339 nm (electronic origin), 327 nm (C−C vibrational shoulder), and 310 nm (weak C−C vibrational shoulder). New absorption features not found in pyrene are the very weak shoulders at 364 and 354 nm. These could arise from electronic transitions that are not present in pyrene itself, be associated with the S_1 state's vibronic structure, or be due to solvent "site broadening". DRF INDOs/CIS computational results presented later in this paper will help distinguish among these possible explanations. The strong absorptions at 278 and 242 nm are typical of electronic absorptions in pyrene. In emission, PAAc has $S_1 \rightarrow S_0$ fluorescence with well resolved C−C vibrational features: 384 nm (electronic origin) followed by vibrational peaks at 404, 426, and 451 nm. One point to stress here is that all four of the emission bands in PAAc correspond to one electronic transition, and they span 80 nm (380−460 nm).

PAdU has spectroscopic features that are very different from those found for PAAc. The increased conjugation in PAdU afforded by changing the methyl group in PAAc to uracil causes a red shift of the initial absorption to ca. 400 nm in the nucleoside from 383 in PAAc. Even more striking in PAdU is that the S_1/S_2 absorption region is now a single broad absorption band with a full width at half-maximum (fwhm) of 56 nm. In emission, the fluorescence region is nearly the mirror image of the absorption region with a 54 nm (fwhm) band. The apparent Stokes shift for these two broad bands is ca. 51 nm (359 → 410 nm) for PAdU, whereas it is at most 1.5 nm for the sharp bands of PAAc. The major electronic difference between PAdU and PAAc is that $Py^{\bullet+}/dU^{\bullet-}$ CT states are present in the nucleoside but absent in PAAc. Whereas broad featureless spectra are common for CT emissions due to strong electronic-librational coupling between the solute and the solvent, sharp vibrational features are characteristic of $^1(\pi,\pi^*)$ emissions from polyaromatic hydrocarbons such as pyrene. Importantly, the CT emission in PAdU extends to 550 nm, whereas the $^1(\pi,\pi^*)$ emission in PAAc ends at 465 nm. However, the (0,0) or origin emission band of PAAc ends at 396 nm (assuming the band is symmetrical).

DRF INDOs/CIS Absorption Spectra for PAAc and PAU_{Me}. Figure 4 presents calculated absorption and density of excited states (DOS) spectra for PAAc (top) and PAU_{Me} (bottom) in MeCN. For PAAc the calculated spectra show weak absorption in the forbidden S_1 region, broad absorption in the S_2 region, and very sharp, strong absorptions around 257 and 236 nm. The first of these appears to be two closely spaced electronic transitions at 258 and 256 nm. Indeed, the second strong absorption band observed experimentally also appears to consist of two closely spaced transitions at 282 and 276 nm. Interestingly, the 4 nm fwhm of the sharp 236 nm band compares very well with the 9 nm fwhm of the origin emission band of PAAc taking account of the fact that the experimental spectrum[1] was broadened with 4 nm wide spectrometer slits, whereas the calculated spectrum was not. Overall the pattern of three regions of strong absorption and one of forbidden absorption found experimentally for PAAc is well reproduced in the calculated absorption spectrum. Importantly, the "extra" broadening in the experimental spectrum of PAAc in its S_2-region (345−370 nm) is very well reproduced by the broad absorption in the S_2-region of the calculated spectrum (320−340 nm). The greatest failing of the DRF INDOs/CIS absorption spectrum of PAAc is that its bands are on average 0.24 (±0.12 std dev) eV blue-shifted with respect to the experimental bands. This failing appears to be due to the earlier noted neglect of dispersion in these calculations.

The top panel in Figure 4 also shows a plot of calculated DOS versus wavelength for PAAc. Although these particular results cannot be compared to a single-photon absorption spectrum, they do show that the electronic manifold of PAAc is much richer than the absorption spectrum alone suggests. In particular, high numbers of forbidden excitations are seen in four regions: 360, 295, 225, and 205 nm.

The bottom panel of Figure 4 shows the calculated absorption spectrum for PAU_{Me} in MeCN. Two features are striking. One,

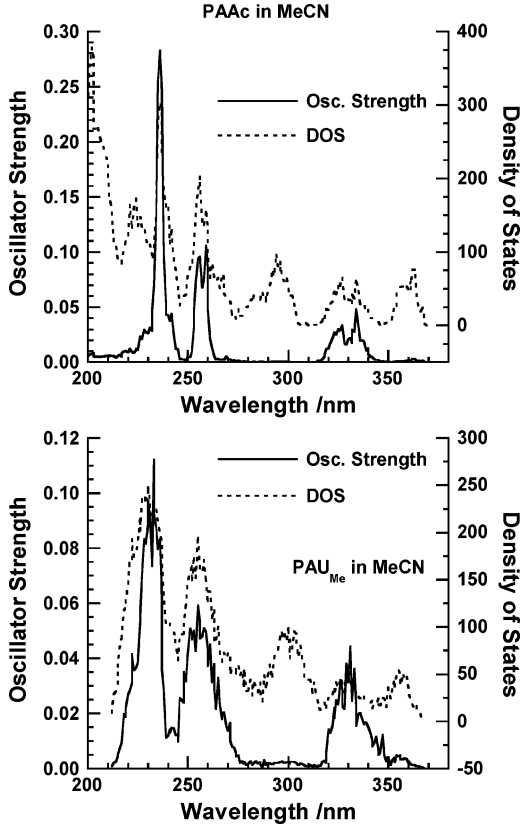

Figure 4. Plots of DRF INDOs/CIS calculated oscillator strength (absorption) versus wavelength and density of excited states (DOS) versus wavelength spectra for PAAc (top) and PAU_{Me} (bottom). Both types of spectra are Boltzmann weighted statistical averages of the individual spectra for eight PAAc or PAU_{Me} conformers each with 100 MeCN configurations. Appropriate Boltzmann factors were calculated on the basis of the relative energy of each solute/solvent configuration. In turn, these relative configuration energies were determined by summing the vacuum ADF energy of the corresponding PAAc or PAU_{Me} conformer with its classical solute configuration energy equilibrated via MD about the charge distribution of the solute's ground state. Spectra were calculated by summing the occurrences of Boltzmann weighted oscillator strength or excited states in each of 200 equal-width energy intervals over the plotted wavelength range.

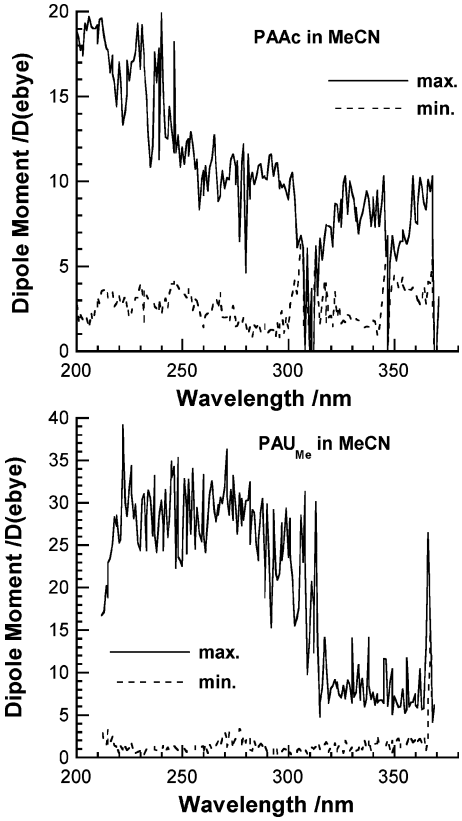

Figure 5. Plots of DRF INDOs/CIS calculated maximum and minimum dipole moment versus wavelength spectra for PAAc (top) and PAU_{Me} (bottom). Each spectrum results from summing individual spectra for eight PAAc or PAU_{Me} conformers each with 100 MeCN solvent configurations equilibrated via MD about the charge distribution of the solute's ground state.

the calculated absorption bands are much broader for PAU_{Me} than for PAAc. This agrees with the experimental absorption spectra for PAdU and PAAc in Figure 3. Two, the absorption bands for PAU_{Me} at 255 and 232 nm are, respectively, about 1.5- and 2.9-fold less intense than the corresponding sharp absorption bands of PAAc. Apparently, the allowed oscillator strength in the sharp bands of PAAc is redistributed among a larger number of states in PAU_{Me}. A similar, but not as large, relative absorption drop is seen in Figure 3 where the ratio of the 242 to 340 nm bands of PAAc is 1.93 but decreases in PAdU to 1.35 for the ratio of the 238 to 358 nm bands. As a result of oscillator strength redistributions on going from PAAc to either PAU_{Me} or PAdU, both pyrenyl-uracil conjugates have absorption spectra with three main bands that are not too different in intensity and that monotonically decrease on going from short to long wavelengths. Importantly, the calculated absorption spectrum of PAU_{Me} has much more intensity in the 340−370 nm region than does the one calculated for PAAc. This result is mirrored experimentally in Figure 3 by the loss of a resolved forbidden band for PAAc on going to PAdU due to much broader absorption in the S_1/S_2-region for PAdU compared to PAAc.

The positions of the three main absorption bands for PAU_{Me} and PAAc in Figure 4 are much the same. This is expected because they would have to shift due to differences in dispersion, and this interaction is neglected here. In fact, the general locations of the bands of PAAc and PAdU do not differ very much. Most of their apparent band shifting is due to two effects: wider absorption bands for PAdU than for PAAc and much more red-edge absorption in the in the S_1/S_2 region for PAdU compared to PAAc, as just noted above.

The bottom panel in Figure 4 shows a plot of calculated DOS and oscillator strength spectra for PAU_{Me}. By comparing these two spectra, high numbers of forbidden excitations can seen to be present in the 360 and 300 nm regions. This is very similar to the DOS and oscillator strength patterns seen in the top panel of Figure 4 for PAAc. For both molecules allowed absorption intensity arises from $\pi \rightarrow \pi^*$ transitions. In PAU_{Me}, $Py^{\bullet+}/dU^{\bullet-}$ CT states can borrow oscillator strength if they are near allowed (π,π^*) states. Oscillator strength borrowing by CT states has two clear consequences for the absorption spectrum of PAU_{Me} compared to that for PAAc. First, it reduces the peak oscillator strengths of the $\pi \rightarrow \pi^*$ transitions in PAU_{Me}. Second, it broadens the width of the absorption bands in PAU_{Me} 2−3-fold compared to the corresponding bands in PAAc.

We just noted large differences in the calculated absorption and DOS spectra for PAU_{Me} versus PAAc in the 220−270 nm region. Figure 5 provides additional insight into the excited states in this region by plotting the spectrum of maximum and minimum dipole moments for both PAAc (top panel) and PAU_{Me} (bottom panel). Note that in both plots the excited states with the largest dipole moments are generally found at the

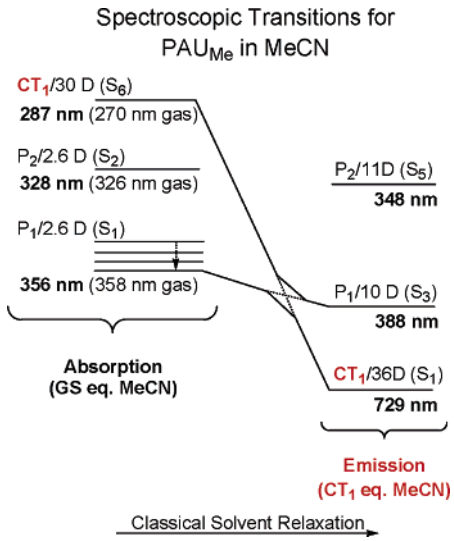

Figure 6. Two electronic transition energy manifolds showing three selected, low energy electronic states (S_n) of a PAU_{Me} conformer in MeCN. (The above data are for conformer E in Mitchell et al.[2] The three configuration defining dihedral angles are the following: (pyrene)-C2−C1−N−H(amide) = −44°, H−N−C−O(amide) = 157°, and (amide)O−C−C5−C4(uracil) = −130°, where a cis dihedral angle is 0° and clockwise rotations of the nearest bond are negative when facing the rotation axis.) Electronic transitions on the left side of the figure have a selected solvent configuration equilibrated via MD about the charge distribution of the ground state (GS eq. MeCN) producing an "absorption manifold"; transitions on the right side have a selected solvent configuration equilibrated via MD about the charge distribution of the lowest-energy, vacuum CT state (CT_1 eq. MeCN) producing an "emission manifold". P_n states correspond to local $^1(\pi,\pi^*)$ excitations of the pyrenyl chromophore. For both the absorption and emission manifolds, separate DRF INDOs/CIS computations yielded the optical transition energies and dipole moment expectation values. For each manifold the illustrated solvent configuration was randomly selected out of 50 000 MD generated solvent configurations using the ground state geometry of conformer E and discrete MeCN molecules both with fixed geometry and atomic charges.

shortest wavelengths. This is reasonable, as the MeCN solvent is equilibrated via MD about the charge distribution of the ground states of the two molecules. Naturally, these "GS equilibrated" solvent configurations are not optimal for excited states with large dipole moments (vertical excitation condition).

Two other aspects of these plots are important. One, the maximum excited state dipole moments are nearly 35 D for PAU_{Me}, whereas they are less than 20 D for PAAc. This is consistent with the largest distance of charge separation in a $Py^{\bullet+}/dU^{\bullet-}$ CT state being greater than the largest charge separation distance possible in an excited state of PAAc. Two, the density of excited states in PAU_{Me} with large dipole moments (25−35 D) is concentrated at wavelengths below 310 nm. This is exactly where we found the largest differences in the calculated absorption and DOS spectra for PAU_{Me} compared to PAAc.

For the vast majority of conformers, the maximum dipole moment plot for PAU_{Me} in Figure 5 suggests that if the MeCN solvent did not fluctuate about the $^1(\pi,\pi^*)$ states of PAdU to lower the energy of $Py^{\bullet+}/dU^{\bullet-}$ CT states, charge separation would not occur. In fact for some conformers of PAdU, CT quenching of their pyrenyl $^1(\pi,\pi^*)$ states takes up to 13 ns. However, for a very high percentage of conformers it occurs in less than 600 fs. Once CT does occur, the solute and solvent can equilibrate about the charge distribution of the new CT state.

Solvent Polarization Effects on Electronic Excited States. Figure 6 illustrates the dramatic effects of equilibrating the solvent to the PAU_{Me} solute with the charge distribution from the first vacuum $Py^{\bullet+}/dU^{\bullet-}$ CT state (CT_1). In particular, the left column of Figure 6 shows the solute's excitation energies (absorption) to three selected excited states and their associated dipole moments for solvent equilibrated about the solute's ground state charge distribution, whereas the right column shows the emission energies and dipole moments of the same three states for solvent equilibrated about the CT_1 state's charge distribution. Note that the two solvent configurations directly influence the solute's electronic properties via separate DRF INDOs/CIS computations. Thus the solute's excited state emission transitions in the right column closely approximate those of a CT excited state (or photoproduct) "in a classically relaxed solvent"; however, the solute itself is not relaxed. Rather the PAU_{Me} conformer in the CT_1 state still has the nuclear configuration of the ground state that it had immediately after photoexcitation. This may be not very important, however, because there is no reason to expect that introducing the effects of solute geometry relaxation would yield very different results from those presented here for the particular excited states involved in this study.

The results illustrated in Figure 6 were obtained for an arbitrary PAU_{Me} conformer (out of the eight conformers examined in this study) and for two arbitrary solvent configurations, one for each of the charge distributions of solute's ground and CT_1 states. According to ADF computations of vacuum energies, the energy of this conformer is 8.4 kcal/mol higher than that of the lowest energy conformer in this study. For clarity in Figure 6, only three of the lowest energy five or six electronic, excited singlet states (P_1, P_2, and CT_1; see the caption in Figure 6 for state definitions) are shown for both absorption and emission in MeCN. Table 1 presents a more complete summary of absorption and emission data for the first seven electronic excited states for the same PAU_{Me} conformer/solvent configurations in Figure 6 including oscillator strengths, optical transition energies, and dipole moments in a vacuum as well as in MeCN.

Two interesting observations can be made on the basis of Figure 6. One, there is almost no absorption energy difference for the P_1, P_2 and CT_1 states on going from a vacuum to MeCN. There likely would be a few more nanometers of red shift for this vacuum to condensed phase change if dispersion effects were calculated. Two, the P_1 and P_2 states increase their dipole moments ca. 8 D and their optical transitions red shift 20−30 nm on going from ground state equilibrated to CT state equilibrated solvent configurations. The most important result, however, is that for the same change of solvent configuration the CT_1 state's emission energy drops dramatically from 287 to 729 nm (2.6 eV!) of which as much as half this drop should be assigned to the upshifting of the ground state energy in its nonequilibrated solvent environment.[31] It is the different charge distributions on the solute in each case that produce the different equilibrated solvent configurations that in turn drive the dramatic differences in the electronic structures of the absorption and emission manifolds of PAU_{Me}.

The data in Table 1 show that absorption to or emission from CT states is strongly forbidden. For example, the CT_1 and CT_2 states in the "MeCN Emission" section of Table 1 are far from the P_1 state (≥0.75 eV) and have oscillator strengths, respectively, of 0.000 02 and 0.000 03. The P_2 state has the largest oscillator strength (0.39), whereas the transition from P_1 is also forbidden (0.0057), but less so than for CT states. The influence of energy proximity on CT state oscillator strength borrowing from an allowed (π,π^*) state can be seen from examination of the data for the CT_4 and CT_5 states. These states are,

TABLE 1: Electronic Properties of the Seven Lowest Energy Excited States of a PAU_{Me} Conformer in Vacuum and in MeCN[a]

excited state number	excited state type[b]	wavelength (nm)	oscillator strength[c]	dipole moment (D)
		Vacuum Absorption[d]		
S_1	P_1	358	0.0089	2.4
S_2	P_2	326	0.65	2.1
S_3	P_3	305	0.016	1.2
S_4	P_4	298	0.018	0.92
S_5	P_5	288	0.0004	2.6
S_6	CT_1	270	0.0012	29.
S_7	P_6	265	0.0010	2.4
		MeCN Absorption[e]		
S_1	P_1	356	0.013	2.6
S_2	P_2	328	0.66	2.6
S_3	P_3	307	0.0044	3.0
S_4	P_4	297	0.041	2.5
S_5	P_5	290	0.0099	2.3
S_6	CT_1	287	0.0017	30.
S_7	P_6	265	0.015	2.8
		MeCN Emission[f]		
S_1	CT_1	729	0.00002	36.
S_2	CT_2	508	0.00003	37.
S_3	P_1	388	0.0057	10.
S_4	CT_3	377	0.045	24.
S_5	P_2	348	0.39	11.
S_6	CT_4	346	0.023	36.
S_7	CT_5	317	0.00061	37.

[a] See Figure 6 and the discussion in the text for a description of the DRF INDOs/CIS and MD computations that the yielded results in this table and Figure 6 for the same two solvent configurations about the PAU_{Me} conformer E from Mitchell et al.[2] [b] P_n and CT_n refer, respectively, to local pyrenyl $^1(\pi,\pi^*)$ and $Py^{\bullet+}/dU^{\bullet-}$ CT excitations. [c] Computed from the DRF INDOs/CIS transition dipole moment for each indicated optical transition. [d] Computed as ground state → excited state vertical excitations of PAU_{Me} conformer E in a vacuum. [e] Computed as ground state → excited state vertical excitations of PAU_{Me} conformer E for a selected, solvent configuration equilibrated about the ground state's charge distribution. [f] Computed as excited state → ground state vertical transitions of PAU_{Me} conformer E for a selected, solvent configuration equilibrated about the vacuum CT_1 state's charge distribution.

respectively, 0.02 and 0.35 eV higher in energy than the strongly allowed P_2 state. Correspondingly, the nearby CT_4 state has oscillator strength of 0.023, whereas the more distant CT_5 state has an oscillator strength of 0.0006. Exceptions to these generalizations can occur when CT states mix strongly with nearby allowed states. For example, the CT_3 state appears to have an anomalously large oscillator strength (0.045) and smaller than expected dipole moment (24 D). Most likely the CT_3 and P_1 states are strongly mixed; together, they appear to have borrowed oscillator strength from the P_2 state. However, an accurate description of the CT_3 and P_1 states likely would require detailed analysis of component orbitals and also likely would not have a simple interpretation.

Note that for PAU_{Me} with CT-equilibrated solvent configurations, the dipole moments of the CT states in Table 1 are ≥24 D, whereas the dipole moments of the local pyrenyl excited states are ≤11 D. The CT-equilibrated emission results in Figure 6 and Table 1 for the selected PAU_{Me} conformer/solvent configuration are qualitatively the similar to the results for the other 99 CT-equilibrated solvent configurations selected from the same large MD run. Quantitatively, some solvent emission configurations have a lower energy CT_1 state, whereas others have a higher energy one. The energy variation with change of solvent configuration for the P_1 and P_2 states is much less than that for the CT states. In emission most solvent configurations produce PAU_{Me} electronic singlet manifolds that have two CT states below the energy of the P_1 state as shown in Table 1, but a few also have either one or three CT states with energies below P_1.

The excited state transition results for PAU_{Me} in Table 1 show that there are no electronic absorptions (i.e., ground state excitations) between P_1 and P_2 in MeCN. This is also true for PAAc. Earlier we discussed possible origins for the very weak, absorption shoulders at 364 and 354 nm for PAAc in Figure 3 that were are not found in pyrene. (An alternate description of these features is the broad, wavy absorption rise in the S_2 region in contrast to the sharp, steep rise seen in this same region in pyrene.) Based on the results in Table 1, these new PAAc absorption features in MeCN cannot be due to electronic transitions that are not present in pyrene. It is possible that they are associated with the P_1 state's vibronic structure, but that is likely to be a minor contribution as P_1 absorption is forbidden in PAAc (see in Figure 4). However, the oscillator strength data in the top panel of Figure 4 also show extensive solvent "site broadening" for PAAc in the P_2 absorption region. Thus, these DRF INDOs/CIS computations clearly demonstrate that the very weak, absorption shoulders at 364 and 354 nm for PAAc in MeCN are due to electronic solute/solvent interactions, very likely involving the amido group of PAAc.

DRF INDOs/CIS Emission Spectra for PAAc and PAU_{Me}. Figure 7 presents in the top panel calculated relative emission spectra in MeCN for PAAc and PAU_{Me} using only the lowest energy excited state and in the bottom panel a calculated relative emission spectrum for PAU_{Me} in the same solvent using the two lowest energy excited states along with the experimental emission spectrum of PAdU in MeCN. The top panel shows that the calculated emission maximum (an apparent electronic origin) of PAAc is 372 nm compared with an experimental electronic origin of 384 nm both in MeCN. The 12 nm discrepancy is likely due to neglect of dispersion in the DRF INDOs/CIS calculation. The calculated emission maximum of PAU_{Me} is at 359 nm, 13 nm to the blue of that for PAAc. For PAdU the electronic origin of emission is difficult to determine but may not differ much from that for PAAc. Future work will have to grapple with how to incorporate dispersion effects for excited states into INDO calculations. The heart of this difficulty is that the INDO basis set is not large enough to simulate the diffuseness of excited state wave functions.

The bottom panel of Figure 7 shows the calculated CT emission spectrum for PAU_{Me} using transitions from the two lowest energy excited states. In this case, the peak emission intensity increases 7.8-fold and shifts to 345 nm from 359 nm compared to emission from only the lowest energy excited state shown in the top panel. There are two reasons why emission from PAdU might reasonably be modeled as originating from the two lowest excited states of PAU_{Me}. First, not all pyrenyl $^1(\pi,\pi^*)$ states in PAdU conformers undergo CT quenching within 600 fs. Thus some PAdU conformers emit from their $^1(\pi,\pi^*)$ state much more strongly than from their CT state. Second, the overall shape of the PAdU emission spectrum is closer to that of PAU_{Me} in the bottom panel than in the top panel. In particular, in the top panel, the relative intensity of PAU_{Me} emission in the 400−600 nm range seems too strong compared to its peak intensity at 359 nm. In the bottom panel, the wider PAdU main emission band (54 nm fwhm) compared to the narrower PAU_{Me} main emission band (14 nm fwhm) likely reflects vibronic contributions that are present in the nucleoside but not in the DRF INDOs/CIS computations for PAU_{Me}. The calculated emission spectra for PAU_{Me} in the top and bottom

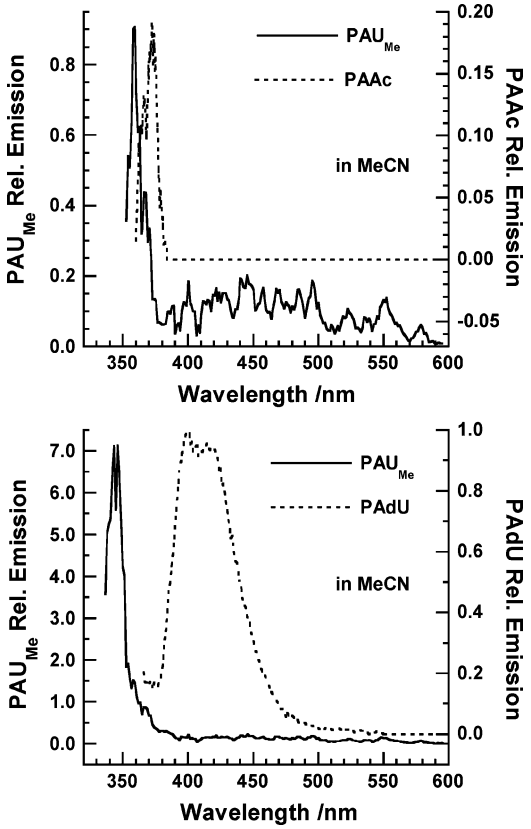

Figure 7. Relative emission spectra in MeCN calculated for both PAU_{Me} and PAAc (top) and calculated for PAU_{Me} and measured for PAdU[1] (bottom). In the figure the calculated spectra for PAU_{Me} and PAAc, respectively, were smoothed over 5 and 2 nm intervals. The calculated emission spectra for PAU_{Me} and PAAc in the top panel were calculated by summing oscillator strengths for the lowest energy excited state over 800 solute/solvent configurations similarly to the summation in Figure 4 but without Boltzmann weighting. As described in Figure 6 for emission spectra, the solvent was equilibrated via MD about the charge distribution of the vacuum CT_1 and P_1 states, respectively, for PAU_{Me} and PAAc. In the bottom panel, the emission spectrum for PAU_{Me} was calculated by summing oscillator strengths for the two lowest energy excited states over 800 solute/solvent configurations.

panels of Figure 7 also show that the greatest density of oscillator strength spans approximately 1.11 eV (the 345−500 nm range). Importantly, Figure 6 and Table 1 also show that thermal solvent fluctuations induce CT_1 emission energies in the 500−726 nm range, but these are judged to make insignificant contributions to emission spectra as they are generally more than 180-fold less intense than the peak emission intensity near 345 nm.

Conclusions

This work models the optical properties of the PAdU nucleoside in polar solvents by calculating the spectral characteristics of a large ensemble of solute/solvent configurations for eight PAU_{Me} conformers in MeCN. It goes beyond an INDOs/CIS SCRF dielectric continuum solvent model by employing explicit MeCN molecules within a discrete reaction field (DRF) solvent model to simulate complete optical band spectra. This approach apart from electrostatic interactions also accounts for many-body polarization interactions and allows for quantitative estimate of the scale of the $Py^{\bullet+}/dU^{\bullet-}$ CT state's emission energy variation that thermal solvent fluctuations can produce. Importantly, it also provides richly detailed results on solvent broadening of optical spectra that is especially important for excited states with large dipole moments in polar solvents.

Comparison of calculated ground state absorption and DOS spectra for PAAc and PA_{Me} shows the presence of large numbers of forbidden optical transitions that cannot be seen in normal (single-photon) optical absorption spectra. The computational results show that peak (π,π^*) absorption oscillator strengths are reduced in PAU_{Me} compared to PAAc and that the allowed absorption bands in PAU_{Me} are 2−3-fold broader than the corresponding bands in PAAc. This latter finding is in excellent agreement with the experimental absorption spectra of PAdU and PAAc in MeCN. Examination of the calculated dipole moments of the excited states produced by light absorption in PAU_{Me} shows that almost all of the large dipole moments ($\geq$25 D) are below 310 nm, i.e., much higher in energy than the lowest energy $^1(\pi,\pi^*)$ state. Thus for the vast majority of PAU_{Me} (and by extension PAdU) conformers, if the MeCN solvent did not fluctuate about their $^1(\pi,\pi^*)$ excited states to lower the energy of their $Py^{\bullet+}/dU^{\bullet-}$ CT states, charge separation would not occur. In fact, for a small fraction of PAdU conformers, CT quenching of their pyrenyl $^1(\pi,\pi^*)$ states takes up to 13 ns. However, for a very large fraction of conformers it occurs in less than 600 fs. The remarkable conclusion is that the time of MeCN reorientation—sufficient to allow CT for most PAdU conformers—is $\leq$600 fs.

Detailed examination of MeCN reorientation results for the $Py^{\bullet+}/dU^{\bullet-}$ CT_1 state of PAU_{Me} for arbitrarily selected conformer/solvent configurations shows two important points. One, solvent reorientation from a ground state equilibrated to a CT state equilibrated configuration lowers the CT_1 state's emission energy to S_0 by 2.6 eV compared to its excitation energy from S_0 (absorption). As much as half of this energy lowering for $CT_1 \rightarrow S_0$ emission comes from destabilization of the ground state. Two, the CT_4 and CT_5 states, respectively 0.02 and 0.35 eV higher in energy than the strongly allowed P_2 state, show clear evidence of energy-proximity dependent emission intensity (oscillator strength) borrowing, respectively, 0.023 and 0.0006. CT emission oscillator strengths when allowed (π,π^*) states are not nearby are very small ($\leq$0.000 03). Last, for CT equilibrated MeCN solvent, the dipole moments of the CT states are generally $\geq$24 D, whereas the dipole moments of the local pyrenyl P_1 and P_2 $^1(\pi,\pi^*)$ states are generally $\leq$11 D.

Very importantly, these explicit solvent DRF computations of the PAU_{Me} model of PAdU reproduce the much broader emission spectra of the nucleoside compared to PAAc. Experimentally, PAdU CT emission in MeCN spans 1.01 eV (380−550 nm); by way of comparison, the calculated CT emission spectrum for the two lowest energy states of PAU_{Me} shows that the greatest density of oscillator strength spans approximately 1.11 eV (345−500 nm). These CT emission calculations also show that thermal solvent fluctuations induce CT_1 emission energies in the 500−726 nm range, but the combination of their low frequency of occurrence and very weak oscillator strengths causes them to make insignificant contributions to CT state emission spectra.

Acknowledgment. We thank the donors of the Petroleum Research Fund, administered by the American Chemical Society, for support of this research. T.L.N. thanks Marla Netzel for assistance with literature research.

References and Notes

(1) Kerr, C. E.; Mitchell, C. D.; Headrick, J.; Eaton, B. E.; Netzel, T. L. *J. Phys. Chem. B* **2000**, *104*, 1637−1650.

(2) Mitchell, C. D.; Netzel, T. L. *J. Phys. Chem. B* **2000**, *104*, 125−136.
(3) Zerner, M. C. Semi Empircal Molecular Orbital Methods. In *Reviews of Computational Chemistry*; Lipkowitz, K. B., Boyd, D. B., Eds.; VCH: New York, 1991; Vol. 2, pp 313−366.
(4) Karelson, M. M.; Zerner, M. C. *J. Phys. Chem.* **1992**, *96*, 6949−6957.
(5) Onsager, L. *J. Am. Chem. Soc.* **1936**, *58*, 1486−1493.
(6) Grozema, F.; Duijnen, P. T. v. *J. Phys. Chem. A* **1998**, *102*, 7984−7989.
(7) Duijnen, P. T. v.; Vries, A. H. d.; Swart, M.; Grozema, F. C. *J. Chem. Phys.* **2002**, *117*, 8442−8453.
(8) Jensen, L.; Duijnen, P. T. v.; Snijders, J. G. *J. Chem. Phys.* **2003**, *119*, 3800−3809.
(9) Jensen, L.; M.Swart; Duijnen, P. T. v. *J. Chem. Phys.* **2005**, *122*, 034103/14.
(10) Grozema, F. C.; Swart, M.; Zijlstra, R. W. J.; Piet, J. J.; Siebbeles, L. D. A.; Duijnen, P. T. v. *J. Am. Chem. Soc.* **2005**, *127*, 11019−11028.
(11) Gaballah, S.; Hussein, Y. H. A.; Anderson, N.; Lian, T. T.; Netzel, T. L. *J. Phys. Chem. A* **2005**, *109*, 10832−10845.
(12) Netzel, T. L.; Nafisi, K.; Headrick, J.; Eaton, B. E. *J. Phys. Chem.* **1995**, *99*, 17948−17955.
(13) Kaden, P.; Mayer-Enthart, E.; Trifonov, A.; Fiebig, T.; Wagenknecht, H.-A. *Angew. Chem., Int. Ed.* **2005**, *44*, 1636−1639.
(14) The longer wavelength of the 590 nm TA maximum of the $Py^{\bullet+}$/$dU^{\bullet-}$ CT state for PdU in phospate buffer compared to the usual TA maximum of the pyrenyl radical cation ($Py^{\bullet+}$) in the 450−460 nm range has been ascribed to electronic coupling (as a result of direct π-orbital overlap) between the radical cation and anion subunits in this state.[13] Similar electronic coupling between the radical subunits in the CT state of PAdU is likely to be responsible for the slightly longer wavelengths of the 520−540 nm TA maxima for PAdU in MeCN and MeOH compared to the usual TA maximum of the pyrenyl radical cation.
(15) Thole, B. T.; Duijnen, P. T. v. *Theor. Chim. Acta* **1980**, *55*, 307−318.
(16) Thole, B. T.; Duijnen, P. T. v. *Chem. Phys.* **1982**, *71*, 211−220.
(17) Vries, A. H. d.; Duijnen, P. T. v.; Juffer, A. H.; Rullmann, J. A. C.; Dijkman, J. P.; Merenga, H.; Thole, B. T. *J. Comput. Chem.* **1995**, *16*, 37−55.
(18) Duijnen, P. T. v.; Grozema, F. C.; Swart, M. *J. Mol. Struct. (THEOCHEM)* **1999**, *464*, 191−198.
(19) Thole, B. T.; Duijnen, P. T. v. *Theor. Chim. Acta* **1983**, *63*, 209−221.
(20) Swart, M.; Duijnen, P. T. v.; Snijders, J. G. *J. Comput. Chem.* **2001**, *22*, 79−88.
(21) Thole, B. T. *Chem. Phys.* **1981**, *59*, 341−350.
(22) Duijnen, P. T. v.; Swart, M. *J. Phys. Chem. A* **1998**, *102*, 2399−2407.
(23) Swart, M.; Duijnen, P. T. v.; Snijders, J. G. *J. Mol. Struct. (THEOCHEM)* **1999**, *458*, 11−17.
(24) Jensen, L.; Åstrand, P.-O.; Osted, A.; Kongsted, J.; Mikkelson, K. V. *J. Chem. Phys.* **2002**, *116*, 4001−4010.
(25) Swart, M.; Duijnen, P. T. v. *Mol. Symm.*, in press.
(26) Ridley, J. E.; Zerner, M. C. *Theor. Chim. Acta (Berl.)* **1973**, *32*, 111−134.
(27) Ridley, J. E.; Zerner, M. C. *Theor. Chim. Acta (Berl.)* **1979**, *42*, 223−236.
(28) Baerends, E. J. Amsterdam Density Functional; Vrje Universiteit, Amsterdam: URL http://www.scm.com.
(29) Toxvaerd, T. *Mol. Phys.* **1991**, *72*, 159−168.
(30) Coutinho, K.; Oliveira, M. J. D.; Canuto, S. *Int. J. Quantum Chem.* **1998**, *66*, 249−253.
(31) Whereas INDOs is parametrized appropriately to simulate absorption and emission spectra, its parameters do not provide reliable ground state energies. Consequently, absolute solvation energies for ground states were not calculated in this work.